Ken'ichiro Yashiro (M'83) was born in Osaka, Japan, on May 5, 1950. He received the B.S. and M.S. degrees in electronic engineering from Chiba University, Chiba, Japan, in 1974 and 1976, respectively, and the Ph.D. degree from Tokyo Institute of Technology, Tokyo, Japan, in 1979.

He joined the Department of Electronic Engineering, Chiba University, as a Research Associate in 1979, and has been engaged in research of acoustic and magnetostatic wave devices.

Dr. Yashiro is a member of the Institute of Electronics and Communication Engineers of Japan.

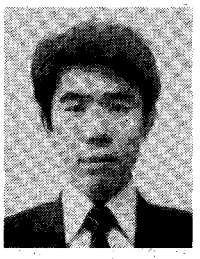

Moriyasu Miyazaki was born in Tokyo, Japan, on July 3, 1959. He received the B.E. degree in electrical engineering and the M.E. degree in electronic engineering from Chiba University, Chiba, Japan, in 1982 and 1984, respectively.

He joined Mitsubishi Electric Corp., Kamakura, Japan, in 1984. He was engaged in the application of MSW to MIC at Chiba University. His current interests are in space communication engineering and electromagnetic wave-scattering problems.

Mr. Miyazaki is a member of the Institute of Electronics and Communication Engineers of Japan.

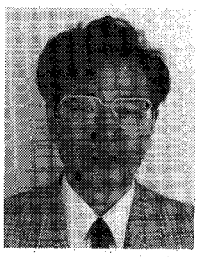

Sumio Ohkawa (M'82–SM'84) was born in Hokkaido, Japan, on July 16, 1935. He received the B.Eng. degree in electrical engineering from Chiba University, Chiba, Japan, in 1961, and the D.Eng. degree from Tokyo Institute of Technology, Tokyo, Japan, in 1974.

He joined the Department of Electrical Engineering of Chiba University as a Research Associate after graduating. In 1970, he transferred to the Department of Electronic Engineering as an Associate Professor, and in 1978 was promoted to full Professor. From October 1979 to June 1980, he studied at the Microwave Research Institute, Polytechnic Institute of New York as a Visiting Professor sent abroad by the Ministry of Education of Japan. His research has chiefly been concerned with measurements of materials in the microwave range. He is now also interested in the applications of magnetostatic waves to microwave integrated circuits.

Dr. Ohkawa is a member of the Institute of Electronics and Communication Engineers of Japan.

Locking Behavior of a Microwave Multiple-Device Ladder Oscillator

SHIGEJI NOGI AND KIYOSHI FUKUI, MEMBER, IEEE

Abstract—**This paper presents a detailed discussion on the injection-locking property of a microwave ladder oscillator which is essentially an array of diode mount-pairs in a rectangular waveguide cavity. It is shown both analytically and experimentally that the use of a ladder structure is advantageous both in obtaining a large locking figure of merit (i.e., $2Q_{ex}^{-1}$) and in rapidity of the transient response to the PSK signal injection.**

I. INTRODUCTION

OWING TO THE increasing demands for high-power microwave generation, various methods have been developed to combine output powers of many active devices. They were well reviewed by K. J. Russel [1] in 1979 and more recently by K. Chang and C. Sun [2] in 1983. In previous papers [3]–[5], the authors proposed a very simple multiple-device structure, i.e., a microwave ladder oscillator, which is essentially an array of diode mount-pairs in a rectangular waveguide, and gave a detailed discussion on the optimum design and successful performance, including a quantitative description of the power-combining mechanism and a mode-analytical discussion of the stable desired-mode operation.

The investigation of the behavior under application of a locking signal must be one of the pertinent problems of such multiple-device oscillators, especially in connection with amplifier application. Kurokawa [6], [7] gave an analytical study using an eigenfunction approach on two multiple-device oscillators of an N-way combining structure (Rucker's [8] and Kurokawa and Magalhaes' [9]). He showed that the locking range and the condition for stable locked operation of such multiple-device oscillators can be given by the expression of the same form as in single-device oscillators, leaving the effect of the number of combined active devices upon the external Q untouched. Experiments on the TM_{ono}-mode cylindrical cavity

Manuscript received February 22, 1984; revised October 30, 1984. This work was supported in part by a Grant in Aid for Fundamental Research from the Ministry of Education, Japan.

The authors are with the Department of Electronics, Okayama University, Okayama 700, Japan.

0018-9480/85/0300-0253$01.00 ©1985 IEEE

combiner [10] and the combiner by Y. E. Ma *et al.* [11], the latter of which is a similar structure to the authors', revealed that the external Q decreases as the number of active devices increases.[1] However, no theoretical description on this effect has been given, as far as the authors know.

The present paper deals with the injection-locking behavior of a microwave ladder oscillator (MLO), and clarifies both by analytical and by experimental study that the use of a ladder structure with several diode mount-pairs is advantageous both in the locking bandwidth and in the rapidity of the transient response to a PSK signal. Section II derives the fundamental equations for discussion of the locking behavior of a MLO based on an equivalent circuit representation. Section III describes the stationary injection-locked state to give a relation of locking bandwidth to circuit parameters, especially to the number of diode mount-pairs. Section IV discusses the transient response to a stepwise (0 to π) phase change of a locking signal by the aid of computer simulation in order to find the dependence of the response speed upon the number of mount-pairs. Last, in Section V, experimental results are presented for comparison with the theoretical ones.

II. Fundamental Equation

A. Equivalent Circuit Representation

The circuit configuration for the injection locking of a microwave ladder oscillator is shown in Fig. 1. An injection signal is introduced through a circulator into the ladder oscillator. Assuming that the waveguide can propagate only the dominant TE_{10} mode, the injection-locking system of Fig. 1 can approximately be represented by Fig. 2(a) using the equivalent circuit given in [5] for the oscillator part. In this figure, $y_{dk} = g_k + jb_{pk}$ is the admittance of the kth mount-pair which includes the diode admittance, package parasitics, and mounting structures[2] (see Fig. 2(b)), and $y_L = g_L + jb_L$ the load admittance looking out at the nth mount-pair (all the admittances are normalized by the characteristic admittance of the waveguide). $\phi_1, \phi_2, \cdots, \phi_N$ denote the electrical length of the relevant waveguide portions.

The locking signal is represented by the current source i_{in} with

$$i_{in} = I_{in}\exp\left[j(\omega_{in}t + \psi_{in})\right]. \tag{1}$$

The available power of the locking signal source is then given by

$$P_{in,a} = I_{in}^2/(8g_L Y_0). \tag{2}$$

In the following sections

$$V_{in} = I_{in}/Y_0 \tag{3}$$

is used instead of I_{in}.

[1] This was also reported in the footnote in [5].

[2] The effects due to interactions among arrays are negligible in the case of $\phi_k \gtrsim 0.26\pi$ at 9.0 GHz in the X-band waveguide, for example, because higher symmetrical modes decay sufficiently.

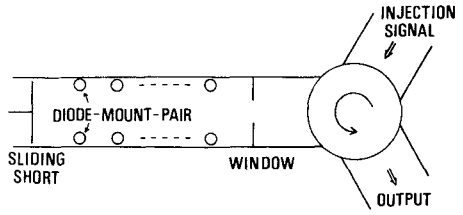

Fig. 1. Injection locking of a microwave ladder oscillator.

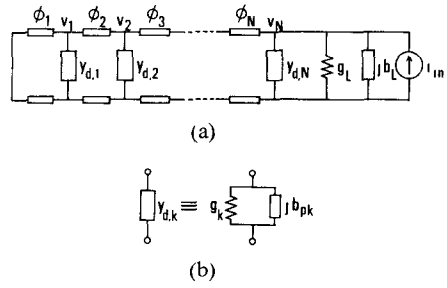

Fig. 2. Equivalent representation for the injection-locked oscillator of Fig. 1; (a) the whole system, (b) the diode mount-pair.

B. Fundamental Equation for Injection Locking

We consider the case in which the frequency of the injection signal ω_{in} is sufficiently close to the free-running oscillation frequency ω_0, and the ladder oscillator is synchronized to the injection signal. Putting

$$v_k = V_k\exp\left[j(\omega_{in}t + \psi_k)\right] \tag{4}$$

we obtain the circuit equations as

$$jb_{tk}V_{k-1}e^{-j\psi_{k,k-1}} + y_kV_k + jb_{t,k+1}V_{k+1}e^{j\psi_{k+1,k}} = \delta_{kN}V_{in}e^{-j(\psi_N - \psi_{in})}, \qquad 1 \leqslant k \leqslant N \tag{5}$$

where

$$\psi_{k,k-1} = \psi_k - \psi_{k-1} \tag{6}$$

$$y_k = (g_k + g_L\delta_{kN}) + jb_k \tag{7}$$

$$b_k = \begin{cases} -\cot\phi_k + b_{pk} - \cot\phi_{k+1}, & 1 \leqslant k \leqslant N-1 \\ -\cot\phi_N + b_{pN} + b_L, & k = N \end{cases} \tag{8}$$

$$b_{tk} = \begin{cases} \operatorname{cosec}\phi_k, & 2 \leqslant k \leqslant N \\ 0, & k = 1,\ N+1. \end{cases} \tag{9}$$

The negative conductance g_k is assumed to have the voltage dependence as

$$g_k(V_k) = -r_k^2 g_{0k} + r_k^4\theta_k V_k^2. \tag{10}$$

$r_k\,(<1)$ represents the coupling reduction which arises because the diode mounts are displaced toward the sidewall of the waveguide.

For a discussion of the injection-locking behavior, V_k and ψ_k must be considered to vary slowly with time. This means that the instantaneous angular oscillation frequency of v_k is given by [12]

$$\omega = \omega_{in} + \frac{d\psi_k}{dt} - j\frac{1}{V_k}\frac{dV_k}{dt}.$$

Then, using a nondimensional time variable $\tau = \omega_0 t$, each admittance in (5) must be described as

$$y_k V_k = \left[y_k|_{\omega=\omega_0} + \tilde{y}_k \left(\delta + \dot{\psi}_k - j\frac{\dot{V}_k}{V_k} \right) \right] V_k, \text{ etc.} \quad (11)$$

where

$$\delta = (\omega_{\text{in}} - \omega_0)/\omega_0 \quad (12)$$

$$\tilde{y}_k = \omega_0 \left. \frac{\partial y_k}{\partial \omega} \right|_{\omega=\omega_0} \quad (13)^3$$

and

$$\dot{V}_k = \frac{dV_k}{d\tau}, \text{ etc.} \quad (14)$$

Substituting (11) into (5), and splitting into the real and imaginary part, we have $2N$ differential equations which describe the locking behavior of a microwave ladder oscillator.

C. Power-Combining Free-Running Operation

Prior to the discussion of the injection locking, power combining at a free-running operation is briefly reviewed. In this section and the following, all the parameters of the diode mount-pairs are assumed to be equal to each other, and the subscript k in g_{0k}, r_k, θ_k, and b_{pk} is omitted.

The basic equations for a steady-state free-running operation can be obtained by putting $V_{\text{in}} = \delta = 0$ and $\dot{V}_k = \dot{\psi}_k = 0$ $(1 \leqslant k \leqslant N)$. It can be shown from these equations that the output power $P_0 = (1/2) g_L Y_0 V_N^2$ reaches the maximum value

$$\max P_0 = N(Y_0/8)\left(g_0^2/\theta\right) \equiv P_{0,0} \quad (15)$$

for

$$V_k^2 = g_0^2/(2r^2\theta) \equiv V_0^2 \quad (16)$$

and

$$g_L = Nr^2 g_0/2 \equiv g_{L,\text{opt}}. \quad (17)$$

Equation (15) indicates that the ladder oscillator is capable of perfect power combining because the available power of each diode mount-pair is given by $(Y_0/8)(g_0^2/\theta)$. Circuit conditions to be satisfied for this power combining, at which the $\psi_{k,k-1}$ value is denoted as $\psi_{k,k-1,0}$, are

$$\left.\begin{aligned} b_{tk} \sin \psi_{k,k-1,0} &= -\frac{1}{2}(k-1) r^2 g_0 \\ b_{tk} \cos \psi_{k,k-1,0} &= \sum_{l=1}^{k-1} (-1)^{k-l} b_l \end{aligned}\right\}, \qquad 2 \leqslant k \leqslant N \quad (18)$$

and

$$\sum_{k=1}^{N} (-1)^k b_k = 0. \quad (19)$$

[3] For example, $\tilde{b}_{tk}$ is given as $\tilde{b}_{tk} = -(v_p/v_g)\phi_k \cot \phi_k \operatorname{cosec} \phi_k$, where v_p and v_g are the phase velocity and the group velocity, respectively, at $\omega = \omega_0$ in the waveguide.

When any two of ω_0, ϕ_1, $\phi_2, \cdots, \phi_N$, and b_L are specified, the remaining circuit parameters and the phase differences between adjacent mount-pairs $\psi_{k,k-1,0}$ $(2 \leqslant k \leqslant N)$ can be determined by use of (18) and (19). A typical optimum design formula for determining the ϕ_k's $(1 \leqslant k \leqslant N)$ and b_L can be derived as [5]

$$\left.\begin{aligned} -\cot \phi_1 &= -\frac{b_p}{2} \\ -\cot \phi_k &= \frac{1}{b_p}\left\{ 1 - \left(\frac{b_p}{2}\right)^2 - \left(\frac{k-1}{2} r^2 g_0\right)^2 \right\}, \end{aligned}\right. \quad (2 \leqslant k \leqslant N) \quad (20)$$

and

$$b_L = -\frac{b_p}{2}.$$

III. Steady-State Injection Locking

In this section, the steady-state response to locking signal injection is investigated. Consider the case where the ladder oscillator to be locked has its maximum output power of (15) before injection. The injection power ratio is, using (2), (3), and $P_{0,0} = \frac{1}{2} g_{L,\text{opt}} Y_0 V_0^2$, given by

$$\frac{P_{\text{in},a}}{P_{0,0}} = \frac{1}{4g_L^2}\left(\frac{V_{\text{in}}}{V_0}\right)^2. \quad (21)$$

A. Case of Double-Diode Oscillator ($N = 1$)

Using subscript s to indicate the quantity at the steady injection-locked state, (5) becomes for the case $N = 1$, using (10), (16), (17), and $b_1 = 0$, which comes from (19)

$$\left\{ g_L\left(\frac{V_{1s}^2}{V_0^2} - 1\right) + \delta(\tilde{g}_1 + \tilde{g}_L) \right\} V_{1s} = V_{\text{in}} \cos \psi_{1s} \quad (22a)$$

$$\delta \tilde{b}_1 V_{1s} = -V_{\text{in}} \sin \psi_{1s} \quad (22b)$$

where $\psi_{\text{in}} = 0$ is assumed. Eliminating ψ_{1s} from both equations in (22), we obtain

$$\left[\left\{ g_L\left(\frac{V_{1s}^2}{V_0^2} - 1\right) + \delta(\tilde{g}_1 + \tilde{g}_L) \right\}^2 + (\delta \tilde{b}_1)^2 \right] \frac{V_{1s}^2}{V_0^2} = \frac{V_{\text{in}}^2}{V_0^2} \quad (23)$$

which gives the response curves in the $\delta - (V_{1s}/V_0)^2$ plane (Fig. 3).

We obtain the conditions for the locking stability by discussing if small disturbances around the steady state $\Delta V_1 = V_1 - V_{1s}$ and $\Delta \psi_1 = \psi_1 - \psi_{1s}$ decay or not with time, by use of (5) with (11), as

$$V_{1s}^2/V_0^2 > 1/2 \quad (24a)$$

$$\left\{ g_L\left(3\frac{V_{1s}^2}{V_0^2} - 1\right) + \delta(\tilde{g}_1 + \tilde{g}_L) \right\} \cdot \left\{ g_L\left(\frac{V_{1s}^2}{V_0^2} - 1\right) + \delta(\tilde{g}_1 + \tilde{g}_L) \right\} + \delta^2 \tilde{b}_1^2 > 0. \quad (24b)$$

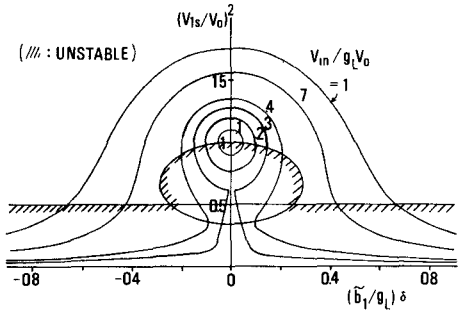

Fig. 3. Response curves and the stable locking region in the $\delta - (V_{1s}/V_0)^2$ plane.

The region of stable locking is also indicated in Fig. 3. As seen in the figure, the region of stable response at small injection power ratio is determined by (24b). It is noted that, just on the boundary of the stable region expressed by (24b), the tangent to the response curve has infinite slope. This means that, for small-signal injection, the point of $dV_{1s}^2/d\delta = \infty$ on a response curve gives the maximum frequency deviation $\delta_{\max}$ and no response can be found beyond $\delta = \delta_{\max}$.

For small values of $|\delta|$, as the border of the stable locking region determined by (24b) is approximated by $V_{1s}^2/V_0^2 > 1 - \{(\tilde{g}_1 + \tilde{g}_L)/g_L\}\delta$, (24b) reduces, using (22a), to

$$\cos\psi_{1s} > 0 \tag{25}$$

which, together with (22b), leads to

$$|\delta_{\max}| = \frac{1}{\tilde{b}_1} \cdot \frac{V_{\text{in}}}{V_0}. \tag{26}$$

Introducing the reciprocal of the gain–bandwidth product at small-signal injection locking Q_{ex} as

$$Q_{\text{ex}} = \lim_{P_{\text{in},a} \to 0} \frac{1}{\delta_{\max}} \sqrt{\frac{P_{\text{in},a}}{P_{0,s0}}} \tag{27}$$

we obtain, using (21) and (26)

$$Q_{\text{ex}} = \frac{\tilde{b}_1}{2g_L} = \frac{\tilde{b}_1}{r^2 g_0} \qquad \text{for } N = 1. \tag{28}$$

B. Case of $N \geq 2$

For the injection-locked ladder oscillator of $N \geq 2$, the steady-state circuit equation is given from (5) by

$$\begin{aligned}&(b_{tk} + \delta\tilde{b}_{tk})V_{k-1,s}\sin\psi_{k'k-1,s} \\ &+ \{g_k + g_L\delta_{kN} + \delta(\tilde{g}_k + \tilde{g}_L\delta_{kN})\}V_{ks} \\ &- (b_{t,k+1} + \delta\tilde{b}_{t,k+1})V_{k+1,s}\sin\psi_{k+1,k,s} = V_{\text{in}}\cos\psi_{Ns}\cdot\delta_{kN}\end{aligned} \tag{29a}$$

$$\begin{aligned}&(b_{tk} + \delta\tilde{b}_{tk})V_{k-1,s}\cos\psi_{k,k-1,s} + (b_k + \delta\tilde{b}_k)V_{ks} \\ &\quad + (b_{t,k+1} + \delta\tilde{b}_{t,k+1})V_{k+1,s}\cos\psi_{k+1,k,s} \\ &\quad = -V_{\text{in}}\sin\psi_{Ns}\cdot\delta_{kN}, \qquad k = 1,2,\cdots,N.\end{aligned} \tag{29b}$$

For small-signal injection, V_{ks} and $\psi_{k,k-1,s}$ are considered to take the values close to those at the free-running operation, and we obtain from (29) the following approximate relations (see Appendix I):

$$\begin{aligned}&b_{tk}\cos\psi_{k,k-1,0}(V_{ks} - V_{k-1,s})/V_0 \\ &\quad = -\delta\left\{\sum_{l=1}^{k-1}\tilde{b}_l + 2\sum_{l=1}^{k-1}\tilde{b}_{tl}\cos\psi_{l,l-1,0} + \tilde{b}_{tk}\cos\psi_{k,k-1,0}\right\}, \\ &\qquad 2 \leq k \leq N\end{aligned} \tag{30}$$

$$\left[\sum_{k=1}^{N}\tilde{b}_k + 2\sum_{k=2}^{N}\tilde{b}_{tk}\cos\psi_{k,k-1,0}\right]\delta = -\frac{V_{\text{in}}}{V_0}\sin\psi_{Ns} \tag{31}$$

$$2g_L\left(\frac{V_{Ns}}{V_0} - 1\right) + \left(\sum_{k=1}^{N}\tilde{g}_k + \tilde{g}_L\right)\delta = \frac{V_{\text{in}}}{V_0}\cos\psi_{Ns}. \tag{32}$$

Equation (30) shows that the amplitude differences between adjacent mount-pairs are proportional to the frequency deviation δ because of the frequency dependence of ϕ_k and b_p. For given V_{in} and δ, the amplitude and the phase at the Nth mount-pairs, V_{Ns} and ψ_{Ns} can be obtained from (31) and (32), and V_{ks} $(1 \leq k \leq N-1)$ can be determined by successive use of (30). Change of $\psi_{k,k-1}$ due to locking is proved to be negligibly small in the present approximation.

Elimination of ψ_{Ns} from (30) and (31) yield

$$\begin{aligned}&\left\{2g_L\left(\frac{V_{Ns}}{V_0} - 1\right) + \left(\sum_{k=1}^{N}\tilde{g}_k + \tilde{g}_L\right)\delta\right\}^2 \\ &\quad + \left\{\sum_{k=1}^{N}\tilde{b}_k + 2\sum_{k=1}^{N}\tilde{b}_{tk}\cos\psi_{k,k-1,0}\right\}^2\delta^2 = \left(\frac{V_{\text{in}}}{V_0}\right)^2\end{aligned} \tag{33}$$

from which again the response curves can be drawn in the $\delta - V_{Ns}$ plane with V_{in} as a parameter. As for the stability of the steady-state solution obtained above, it is not so easy to find an analytical expression using the Routh–Hurwitz criterion as it was in the case $N = 1$. However, by use of a tentative criterion discussed in Section III-A that the border of the stable locking region satisfies $dV_{Ns}/d\delta = \infty$ for small-signal injection, we have $\psi_{Ns} = \pm\pi/2$ on the border from (32) and (33). This leads, together with the use of (31) and (18), to

$$\delta_{\max} = \left[\sum_{k=1}^{N}\tilde{b}_k + 2\sum_{k=2}^{N}\frac{\tilde{b}_{tk}}{b_{tk}}\left\{\sum_{l=1}^{k-1}(-1)^{k-l}b_l\right\}\right]^{-1}\frac{V_{\text{in}}}{V_0}. \tag{34}$$

Further, by use of (27), (21), (17), and (34), we finally obtain

$$Q_{\text{ex}} = \frac{1}{Nr^2 g_0}\left[\sum_{k=1}^{N}\tilde{b}_k + 2\sum_{k=2}^{N}\frac{\tilde{b}_{tk}}{b_{tk}}\left\{\sum_{l=1}^{k-1}(-1)^{k-l}b_l\right\}\right]. \tag{35}$$

For a ladder oscillator of typical design (20), use of (35) shows that Q_{ex} markedly decreases with increasing N for low numbers of N, as shown in Fig. 4.

A physical explanation for (35) and Fig. 4 is given in Appendix II.

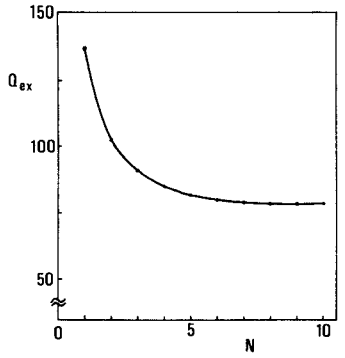

Fig. 4. Calculated Q_{ex} values for microwave ladder oscillators of typical design ($r^2 g_0 = 0.15$, $b_p = -1.5$, $\tilde{b}_p = 6.0$, $\omega_0/2\pi = 9.0$ GHz).

C. Effect of Voltage Dependence of the Diode Susceptance

In the case when the voltage dependence of b_p has to be considered, we can also obtain the theoretical expression for Q_{ex} in the same way as discussed above (Appendix III):

$$Q_{ex} = \frac{1}{2g_L} \cdot \frac{\left| 2g_L B_N - A_N \left(\sum_{k=1}^{N} \tilde{g}_k + \tilde{g}_L \right) \right|}{\sqrt{(2g_L)^2 + A_N^2}} \quad \text{for } N \geqslant 1 \tag{36}$$

where, putting $\tilde{\tilde{b}}_p \equiv V_0 [\partial b_p / \partial V]_{V=V_0}$

$$A_1 = b_1 + \tilde{\tilde{b}}_p$$

$$B_1 = \tilde{b}_1 + \tilde{b}_{t2} \cos \psi_{21,0}$$

$$A_k = b_k + \tilde{\tilde{b}}_p - \frac{(b_{tk} \cos \psi_{k,k-1,0})^2}{A_{k-1}}$$

$$B_k = \left(-\frac{B_{k-1}}{A_{k-1}} + \frac{\tilde{b}_{tk}}{b_{tk}} \right) b_{tk} \cos \psi_{k,k-1,0} + \tilde{b}_k + \tilde{b}_{t,k+1} \cos \psi_{k+1,k,0}, \qquad 2 \leqslant k \leqslant N. \tag{37}$$

Later in Section V, calculated values of Q_{ex} by (36) are plotted in Fig. 12.

IV. Transient Response

In recent years, PCM-PM transmission systems have been occupying a larger part in microwave communications. For the purpose of applying the injection locking of microwave ladder oscillators to amplification of a PCM-PM signal, let us consider the transient response of a ladder oscillator to a PSK signal injection.

A. Transient Response of a Double-Diode Oscillator ($N = 1$)

The transient response of an injection-locked double-diode oscillator ($N=1$) with no voltage dependence of diode susceptance is described from (5) by, when $\psi_{in} = 0$ is assumed

$$\frac{dV_1}{d\tau} = \frac{V_{in}}{Q_1} \cos(\psi_1 - \alpha_1) - \frac{V_1}{Q_1^2} g_L \tilde{b}_1 \left(\frac{V_1^2}{V_0^2} - 1 \right) \tag{38a}$$

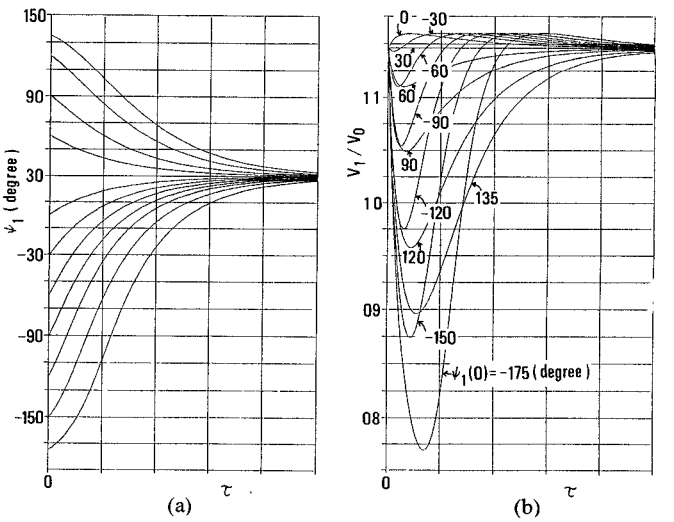

Fig. 5. Transient response of a double-diode oscillator ($N=1$) for various initial phase differences ($r^2 g_0 = 0.15$, $\tilde{b}_1 = 30$, $\tilde{g}_1 + \tilde{g}_L = 2$, $P_{in,a}/P_{0,0} = 0.04$). (a) Phase response. (b) Amplitude response.

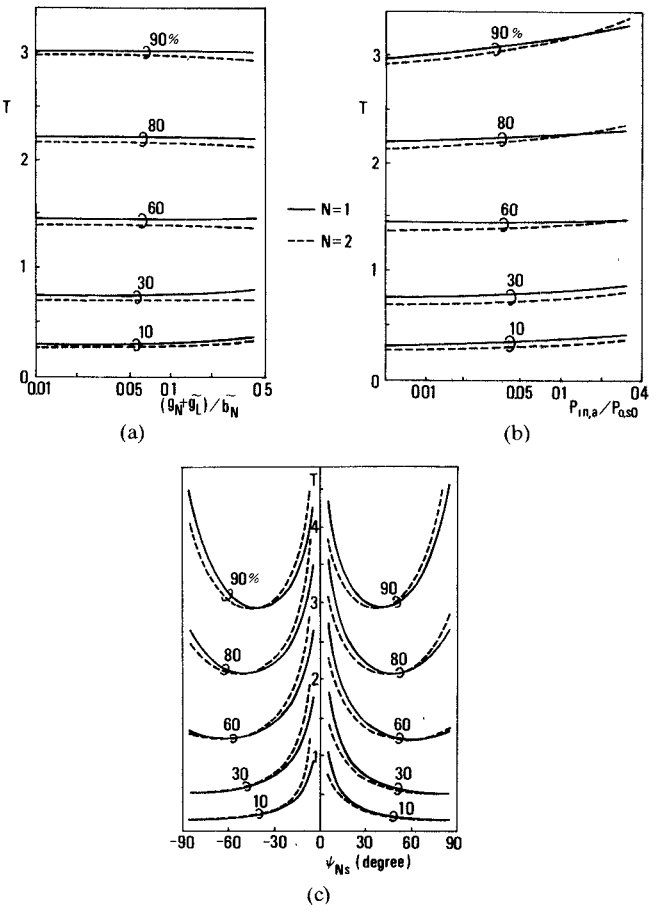

Fig. 6. Parameter dependency of the transient response in case of $N=1$ (solid lines) and $N=2$ (dashed lines); T_x is the normalized time which corresponds to x percent of the total phase change. (a) $(\tilde{g}_N + \tilde{g}_L)/\tilde{b}_N$, (b) $P_{in,a}/P_{0,0}$, (c) ψ_{Ns}.

$$\frac{d\psi_1}{d\tau} = -\frac{V_{in}}{Q_1 V_1} \sin(\psi_1 - \alpha_1) - \delta - \frac{1}{Q_1^2} g_L (\tilde{g}_1 + \tilde{g}_L) \cdot \left(\frac{V_1^2}{V_0^2} - 1 \right) \tag{38b}$$

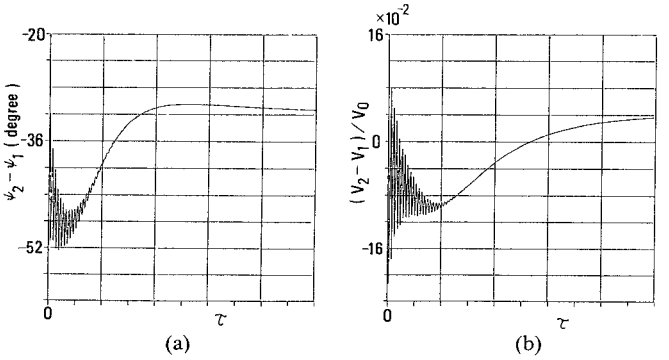

Fig. 7. Transient response ($N=2$, $P_{in,a}/P_{0,0}=0.02$). (a) $\psi_2-\psi_1$, (b) $(V_2-V_1)/V_0$.

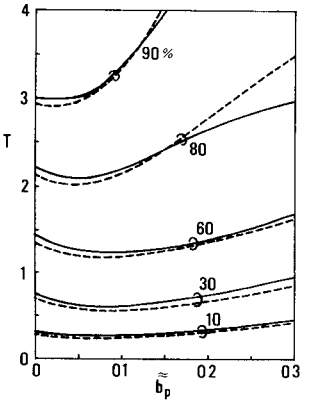

Fig. 8. Effect of $\tilde{b}_p$ on the transient response in case of $N=1$ (solid lines) and $N=2$ (dashed lines).

where

$$\left.\begin{aligned} Q_1 &= \sqrt{\tilde{b}_1^2+(\tilde{g}_1+\tilde{g}_L)^2} \\ \alpha_1 &= \tan^{-1}\frac{\tilde{g}_1+\tilde{g}_L}{\tilde{b}_1} \end{aligned}\right\}. \tag{39}$$

It can be shown from (38) using (21), (28), and $T=\delta_{\max}\tau$ that the transient response with respect to the normalized time variable T depends upon the parameters α_1, $P_{in,a}/P_{0,0}$, ψ_{1s}, and the initial phase difference $\psi_1(0)$ but not upon g_L nor Q_1. The responses for various $\psi_1(0)$'s obtained by computer simulation are shown in Fig. 5. When $\cos(\psi_1(0)-\alpha_1)<\cos(\psi_{1s}-\alpha_1)$, V_1 decreases at an early stage, which accelerates the time variation of ψ_1. An abrupt phase change from $-\pi$ to 0 in the injected signal causes a variation of ψ_1 from $\psi_{1s}-\pi$ to ψ_{1s}. A normalized time T_x which corresponds to x percent of the total phase change is plotted for several values of x in Fig. 6.[4] Defining the rise time of ψ_1 by $T_r=T_{90}-T_{10}$, we can see from Fig. 6 that T_r is almost independent of α_1 and $P_{in,a}/P_{0,0}$. The independence of T_r means that the rise time is inversely proportional to the locking bandwidth.

B. Transient Response in a Quadruple-Diode Oscillator ($N=2$)

The transient response of a quadruple-diode oscillator is described from (15) by

$$\begin{pmatrix} \tilde{b}_1 & \tilde{g}_1 & \tilde{b}_{t2}\cos\psi_{21} & -\tilde{b}_{t2}\sin\psi_{21} \\ -\tilde{g}_1 & \tilde{b}_1 & \tilde{b}_{t2}\sin\psi_{21} & \tilde{b}_{t2}\cos\psi_{21} \\ \tilde{b}_{t2}\cos\psi_{21} & \tilde{b}_{t2}\sin\psi_{21} & \tilde{b}_2 & \tilde{g}_2+\tilde{g}_L \\ -\tilde{b}_{t2}\sin\psi_{21} & \tilde{b}_{t2}\cos\psi_{21} & -(\tilde{g}_2+\tilde{g}_L) & \tilde{b}_2 \end{pmatrix}\begin{pmatrix} \dot{V}_1 \\ V_1\cdot\dot{\psi}_1 \\ \dot{V}_2 \\ V_2\cdot\dot{\psi}_2 \end{pmatrix}$$

$$=\begin{pmatrix} 0 \\ 0 \\ V_{in}\cos\psi_2 \\ -V_{in}\sin\psi_2 \end{pmatrix}-\begin{pmatrix} (g_1+\delta\tilde{g}_1)V_1-(b_{t2}+\delta\tilde{b}_{t2})V_2\sin\psi_{21} \\ (b_1+\delta\tilde{b}_1)V_1+(b_{t2}+\delta\tilde{b}_{t2})V_2\cos\psi_{21} \\ (b_{t2}+\delta\tilde{b}_{t2})V_2\sin\psi_{21}+\{g_2+g_L+\delta(\tilde{g}_2+\tilde{g}_L)\}V_2 \\ (b_{t2}+\delta\tilde{b}_{t2})V_2\cos\psi_{21}+(b_2+\delta\tilde{b}_2)V_2 \end{pmatrix}. \tag{40}$$

[4] In Figs. 6–8, computer simulations were carried out using the following typical parameter values unless otherwise specified; $P_{in,a}/P_{0,s0}=0.01$, $g_L=0.075\times N$, $\tilde{b}_p=0$, $\psi_{Ns}=30°$ together with $\tilde{b}_1=30$ and $\tilde{g}_1+\tilde{g}_L=2$ for $N=1$ and $\tilde{b}_1=10$, $\tilde{g}_1=0.1$, $\tilde{b}_2=30$, $\tilde{g}_2+\tilde{g}_L=3$, $b_1=b_2=-1.05$, $b_{t2}=1.05$ and $b_{t2}=-0.644$ for $N=2$.

Simulation of (40) gives almost the same transient responses for ψ_2 and V_2 as those for ψ_1 and V_1 in a double-diode oscillator. The differences $\psi_2-\psi_1$ and V_2-V_1 are shown in Fig. 7; the deviations from their steady-state values are considerably small. Fig. 6 shows the parameter dependence of the transient response of a quadruple-diode oscillator into which a bi-phase PSK signal is injected. We find from this figure that the normalized rise time T_r of ψ_2 is almost independent of the parameters except ψ_{2s} and is almost equal to that of a double-diode oscillator.

Under the same injection power ratio, the rise time for $N=2$ is less than that for $N=1$ because the locking bandwidth is wider in the former than the latter, as shown in Fig. 4.

C. Effect of Voltage-Amplitude Dependence of the Diode Susceptance

The transient response is rather complicated when the voltage-amplitude dependence of the diode susceptance must be considered.

The response of a double-diode oscillator when $b_p\neq 0$ is given by (38a) and (38b) with additions of $(\tilde{g}_1+\tilde{g}_L)\tilde{b}_p(V_1/V_0)(V_1/V_0-1)/Q_1^2$ and $-\tilde{b}_1\tilde{b}_p(V_1/V_0-1)/Q_1^2$ to their right-hand sides, respectively. Accordingly, in the case of $\tilde{b}_1\tilde{b}_p>0$, the voltage-amplitude dependence has the effect of accelerating the time variation of ψ_1 when $V_1/V_0<1$ and decelerating when $V_1/V_0>1$. Fig. 8 shows the response of ψ_1 under a bi-phase PSK signal injection. The larger is $\tilde{b}_p$ (i.e., the smaller is Q_{ex}), the smaller becomes the rise time.

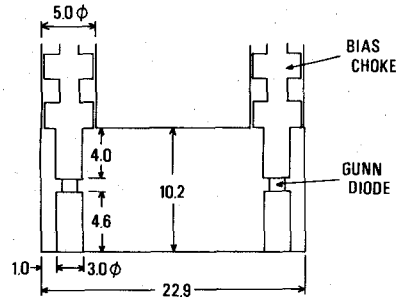

Fig. 9. Configuration of a diode mount-pair module (all dimensions are in millimeters).

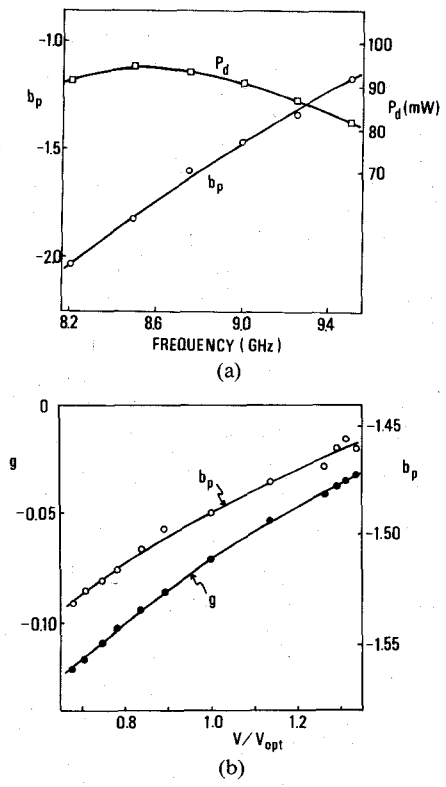

Fig. 10. Typical characteristics of a diode mount-pair. (a) Frequency dependence of b_p and the maximum output power P_d. (b) Voltage-amplitude dependence of b_p and the negative conductance g at 8.95 GHz. In Fig. (a), the b_p values were obtained by substituting the value of b_L and ϕ_1, which are measured in the maximum output power generation of the double-diode oscillator with the diode mount-pair, into the oscillation condition $-\cot\phi_1 + b_p + b_L = 0$ at each oscillation frequency. Fig. (b) was obtained from the measured values of the output power P_0 and the load admittance $g_L + jb_L$ of the double-diode oscillator for various load adjustments under the constant oscillation frequency; the voltage amplitude V is calculated using $P_0 = 1/2 g_L Y_0 V^2$, and g is obtained as $g = -g_L$.

The response of a quadruple-diode oscillator is described by (40) in which b_k is replaced by $b_k|_{V_k=V_0} + \tilde{b}_p(V_k/V_0 - 1)$, $(k = 1, 2)$. As seen in Fig. 8, for small-signal injection, the effect of $\tilde{b}_p$ to the response of the output voltage phase in $N = 2$ is almost equal to that in $N = 1$ so long as $\tilde{b}_p$ is small.

V. Experimental Results

Injection-locking experiments were carried out for X-band oscillators with up to four diode mount-pairs using Gunn diodes GD511A manufactured by the Nippon Electric Company. The configuration of a diode mount-pair module is shown in Fig. 9. The characteristics of the four mount-pairs used were considerably close to each other. Fig. 10 shows typical data; the average values were $r^2 g_0 = 0.142$, $b_p = -1.45$, $\tilde{b}_p = 5.75$, and $\tilde{\tilde{b}}_p = 0.090$ at $f = 8.95$ GHz.

The ladder oscillators were designed using (17) and (20) so that it can generate the maximum output power in free-running oscillation at 8.95 GHz. A three-stub tuner is placed next to the coupling iris to make fine adjustments of the load admittance. The oscillator thus constructed was adjusted to maximize the output power at the given oscillation frequency using the sliding short and the three-stub tuner.

Fig. 11 shows the experimental result of the relation between the injection power ratio and the locking range. The experimental Q_{ex} values of the oscillators obtained from Fig. 11 are plotted in Fig. 12. In Fig. 12, the theoretical Q_{ex} values are also plotted for comparison, which were

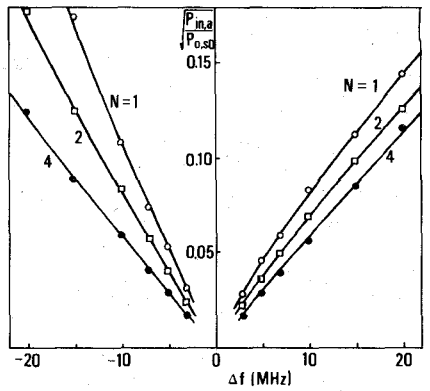

Fig. 11. Measured locking range ($f_0 = \omega_0/2\pi = 8.95$ GHz).

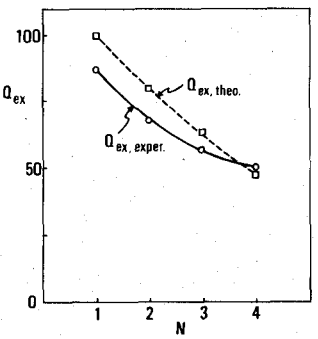

Fig. 12. Q_{ex} values of ladder oscillators.

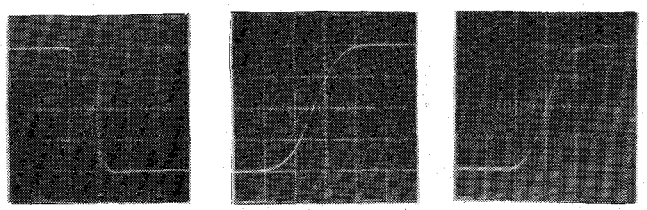

Fig. 13. Transient phase response. (a) Injected PSK signal. (b) Output PSK signal ($N = 1$). (c) Output PSk signal ($N = 4$).

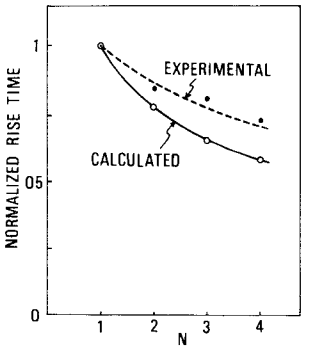

Fig 14. Rise time of the phase response

calculated from (36) using the data of the diode mount-pairs and the measured values of the circuit parameters. It can be seen in Fig. 12 that the experimental Q_{ex} values are in fair agreement with the theoretical ones. The power-combining efficiencies of the ladder oscillators used for experiments were above 95 percent.

The transient phase responses of ladder oscillators to the injection of the bi-phase PSK wave generated using a p-i-n modulator are given in Fig. 13, where PSK signals detected by a phase discriminator are shown. The measured rise time of the phase response can be obtained from the observed data as shown in Fig. 13 taking account of the rise time of the oscilloscope (7 ns) used in the experiment. A result for $P_{in,a}/P_{0,0} = 0.002$ and $\delta = -(1/2)\delta_{max}$ is plotted in Fig. 14, where rise times are normalized by the rise time of a double-diode oscillator ($N = 1$).

From the theoretical result of the foregoing section, a ladder oscillator can be considered to have almost the same rise time as the double-diode oscillator with an equal locking range and frequency deviation. In order to obtain the rise time theoretically, we assume that the crystal detector of the phase discriminator has the characteristic of square voltage dependence, and take account of the rise time of the incoming bi-phase PSK wave. Representing the incoming wave as $V_{in}(t)\cos\{\omega_{in}t + \psi_{in}(t)\}$ with appropriate time functions $V_{in}(t)$ an $\psi_{in}(t)$ to give the output waveform of the phase discriminator for the incoming wave observed in the experiment, we obtained the output waveform of the phase discriminator for the injection-locked oscillator output by the computer simulation of (38) supplemented to contain the effects of $\tilde{b}_p$, $V_{in}(t)$ and $\psi_{in}(t)$. The result is also shown in Fig. 14. The ratio of the experimental value of the rise time for $N = 1$ to the calculated one in Fig. 14 was 0.66. We can see in Fig. 14 the qualitative agreement between the experimental and the calculated result. Accordingly, it can be said both theoretically and experimentally that the injection-locked ladder oscillator with larger N has wider locking range and faster transient response.

VI. Conclusion

We have discussed both the steady-state and the transient response of an injection-locked microwave ladder oscillator.

The expression for the reciprocal of the gain–bandwidth product, that is, for Q_{ex} has been derived for small-signal injection. The measured Q_{ex} values were in fairly good agreement with the theoretical ones for the oscillators with up to eight Gunn diodes. It can be shown that Q_{ex} greatly decreases with an increasing number of the diode mount-pairs N for low N. Because of fairly good agreement between the theoretical and the experimental results, the criterion used in the discussion of locking stability is considered reasonable, which states that the tangent of the response curve has the infinite slope just on the border of the stable locking region for small-signal injection.

As for the transient response of a ladder oscillator to the PSK signal injection, numerical investigation has shown that the rise time in the phase response of the oscillator is almost in inverse proportion to the locking range. This result was confirmed by experiment for $N \leqslant 4$.

All the results in this paper may ensure that the injection locking of a ladder oscillator is useful for microwave amplification of high output power in both FM and PCM-PM transmission systems. While, in this paper, the locking behavior for small-signal injection has mainly been discussed, the case for large-signal injection remains for future study.

Appendix I
Derivation of (30) ~ (32)

For small-signal injection, expressing $V_{ks} = V_0 + \Delta V_{ks}$ and $\psi_{k+1,k,s} = \psi_{k+1,k,0} + \Delta\psi_{k+1,k,s}$, where ΔV_{ks} and $\Delta\psi_{k+1,k,s}$ are the deviations from the free-running solutions, we can expect all of V_{in}/V_0, δ, $\Delta V_{ks}/V_0$ and $\Delta\psi_{k+1,k,s}$ to be of the order of a small quantity, ϵ_1. Substituting these expressions into (29) and discarding the second-order terms $0(\epsilon_1^2)$ gives

$$\begin{aligned}&\delta\tilde{b}_{t,l}\sin\psi_{l,l-1,0} + b_{t,l}\sin\psi_{l,l-1,0}\cdot\Delta V_{l-1,s}\\&\quad + b_{t,l}\cos\psi_{l,l-1,0}\cdot\Delta\psi_{l,l-1,s} - g_{opt}\Delta V_{ls} + \delta(\tilde{g}_l + \tilde{g}_l\delta_{kN})\\&\quad - \delta\tilde{b}_{t,l+1}\sin\psi_{l+1,l,0} - b_{t,l+1}\sin\psi_{l+1,l,0}\cdot\Delta V_{l+1,s}\\&\quad - b_{t,l+1}\cos\psi_{l+1,l,0}\cdot\Delta\psi_{l+1,l,s} = V_{in}\cos\psi_{N,s}\cdot\delta_{lN} \qquad (41a)\end{aligned}$$

$$\begin{aligned}&\delta\tilde{b}_{t,l}\cos\psi_{l,l-1,0} + b_{t,l}\cos\psi_{l,l-1,0}\cdot\Delta V_{l-1,s}\\&\quad - b_{t,l}\sin\psi_{l,l-1,0}\cdot\Delta\psi_{l,l-1,s} + b_l\cdot\Delta V_{l,s} + \delta\tilde{b}_l\\&\quad + \delta\tilde{b}_{t,l+1}\cos\psi_{l+1,l,0} + b_{t,l+1}\cos\psi_{l+1,l,0}\cdot\Delta V_{l+1,s}\\&\quad - b_{t,l+1}\sin\psi_{l+1,l,0}\cdot\Delta\psi_{l+1,l,s} = -V_{in}\sin\psi_{N,s}\cdot\delta_{lN},\\&\qquad 1 \leqslant l \leqslant N \qquad (41b)\end{aligned}$$

where $g_{opt}(= -(1/2)r^2g_0)$ is the g_k value at the free-running oscillation.

On the other hand, for small coupling reduction, we find from (10) and (18) that g_{opt}, $\tilde{g}_l$, and $b_{tl}\sin\psi_{l,l-1,0}$ are of the order of another small quantity, say, ϵ_2.

For injection of such a small signal that satisfies $\epsilon_1 = 0(\epsilon_2^2)$, (41a) gives a result that $\Delta\psi_{l,l-1,s}(2 \leqslant l \leqslant N)$ is of the order of ϵ_2^3, which permits discarding terms such as $b_{t,l}\sin\psi_{l,l-1,0}\cdot\Delta\psi_{l,l-1,s}$ in (41b). Adding all of (41b) with $l = 1,2,\cdots,k$ yields (30) using (18). Similarly, (41b) with $l = 1,2,\cdots,N$, each multiplied by $(-1)^{N-l}$, gives (31) using (18) and (30), while (41a) leads to (32) using (18).

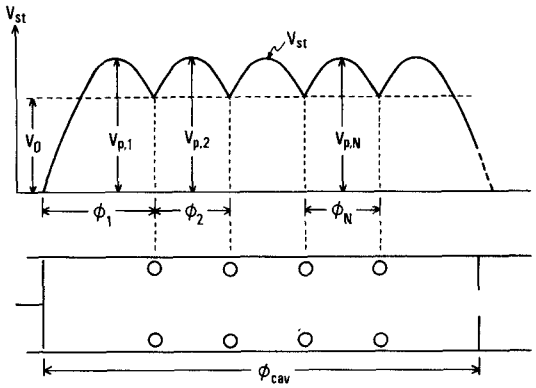

Fig. 15. Voltage standing wave in a microwave ladder oscillator of power-combining design.

Appendix II
Physical Explanation for Q_{ex} of the Ladder Oscillator

Equation (35) can be written using (31), (17), and (18) as $Q_{ex} = \tilde{B}/(2g_L)$, where B is the susceptance looking toward the ladder oscillator from the injection current source i_{in} in Fig. 2(a).

On the other hand, denoting the stored energy in the resonant cavity and the dissipated power in the output line as W and P_0, respectively, the fundamental definition of Q_{ex} is given by

$$Q_{ex} = \omega_0 W/P_0. \tag{42}$$

It can be clarified that the right side of (42) is equal to $\tilde{B}/(2g_L)$ [13].

Fig. 15 shows the amplitude of the voltage standing wave V_{st} in the resonant cavity of the ladder oscillator in the perfect power-combining operation [5]. In the case of $r^2 g_0 N \ll 1$, (20) can be approximated as

$$\phi_k = \cot^{-1}\left[-\frac{1}{b_p}\left\{1-\left(\frac{b_p}{2}\right)^2\right\}\right] \equiv \phi^{(0)}, \qquad k \geqslant 2 \tag{43}$$

and V_{st} takes the peak value

$$V_{p,k} = V_0 \sec\frac{\phi^{(0)}}{2} \equiv V_p^{(0)}. \tag{44}$$

The energy stored in the cavity of electric length ϕ_{cav} is obtained as

$$W = A\int_0^{\phi_{cav}} V_{st}^2\, d\phi$$
$$= AV_p^{(0)2}\left\{\pi + N\left(\phi^{(0)} + \sin\phi^{(0)}\right)\right\} \tag{45}$$

where A is a constant. As the dissipated power is given from (16) and (17) by $P_0 = (Y_0/2)g_{L,opt}V_N^2 = (Y_0/4)Nr^2 g_0 V_0^2$, we obtain Q_{ex} of the ladder oscillator with N mount-pairs as

$$Q_{ex}(N) = \frac{4\omega_0 A}{Y_0 r^2 g_0}\cdot\frac{\pi + N\left(\phi^{(0)} + \sin\phi^{(0)}\right)}{N\cot^2\left(\phi^{(0)}/2\right)}. \tag{46}$$

Accordingly

$$\frac{Q_{ex}(N)}{Q_{ex}(1)} = \frac{1}{\pi + \phi^{(0)} + \sin\phi^{(0)}}\left(\frac{\pi}{N} + \phi^{(0)} + \sin\phi^{(0)}\right) \tag{47}$$

which shows that Q_{ex} decreases with increasing N as in Fig. 4.

Appendix III
Derivation of (36)

When the voltage-amplitude dependence of b_p is considered, b_k in (29) must be replaced by $b_k|_{V_{ks}=V_0} + \tilde{b}_p(V_{ks}/V_0 - 1)$. Putting $V_{ks} = V_0 + \Delta V_{ks}$ and $\psi_{k+1,k,s} = \psi_{k+1,k,0} + \Delta\psi_{k+1,k,s}$ in the same way as in Appendix I, and neglecting the second-order term $0(\epsilon_1^2)$, we obtain the modified equations (41b) with addition of $\tilde{b}_p \Delta V_{ls}$ to their right-hand sides, leaving (41a) unchanged.

Successive elimination of $\Delta V_{ls}(l = 1,2,\cdots,k-2)$ from the modified (41b) with $l = 2,3,\cdots,k-1$ yields

$$\left(A_{k-1}\cdot\Delta V_{k-1,s} + b_{tk}\cos\psi_{k,k-1,0}\cdot\Delta V_{k,s}\right)/V_0 + B_{k-1}\delta = 0,$$
$$k = 2,3,\cdots,N \tag{48}$$

where A_k and B_k are obtained from (37). Elimination of $\Delta V_{N-1,s}$ from modified (41b) with $l = N$ and (48) with $k = N$ gives

$$A_N\cdot\Delta V_{N,s}/V_0 + B_N\delta = -(V_{in}/V_0)\sin\psi_{N,s}. \tag{49}$$

Equations (48) and (49) reduce to (30) and (31), respectively, in the case of $\tilde{b}_p = 0$. Equation (32) holds also in the case of $\tilde{b}_p \neq 0$. Equations (49) and (32) lead to (36) in the same way as in Section III-B.

Acknowledgment

The authors wish to thank N. Ohmoto and S. Tanaka for their invaluable assistance, especially in carrying out the experiments and the computer work.

References

[1] K. Russel, "Microwave power combining techniques," *IEEE Trans. Microwave Theory Tech.*, vol. MTT-27, pp. 472–477, May 1979.
[2] K. Chang and C. Sun, "Millimeter-wave power-combining techniques," *IEEE Trans. Microwave Theory Tech.*, vol. MTT-31, pp. 91–107, Feb. 1983.
[3] K. Fukui and S. Nogi, "Power combining ladder network with many active devices," *IEEE Trans. Microwave Theory Tech.*, MTT-28, pp. 1059–1067, Oct. 1980.
[4] K. Fukui and S. Nogi, "A microwave multiple-diode ladder oscillator," *Trans. IECE Japan*, vol. J64-B, pp. 816–823, Aug. 1981.
[5] S. Nogi and K. Fukui, "Optimum design and performance of a microwave ladder oscillator with many diode mount pairs," *IEEE Trans. Microwave Theory Tech.*, vol. MTT-30, pp. 735–743, May 1982.
[6] K. Kurokawa, "The single-cavity multiple-device oscillator," *IEEE Trans. Microwave Theory Tech.*, vol. MTT-19, pp. 793–801, Oct. 1971.
[7] K. Kurokawa, "Injection locking of microwave solid-state oscillators," *Proc. IEEE*, vol. 61, pp. 1386–1410, Oct. 1973.
[8] C. T. Rucker, "A multiple-diode high-average-power avalanche-diode oscillator," *IEEE Trans. Microwave Theory Tech.*, vol. MTT-17, pp. 1156–1158, Dec. 1969.
[9] K. Kurokawa and F. M. Magalhaes, "An *X*-band 10-watt multiple-IMPATT oscillator," *Proc. IEEE* vol. 59, pp. 102–103, Jan. 1971.
[10] R. Aston, "Techniques for increasing the bandwidth of a TM_{010}-mode power combiner," *IEEE Trans. Microwave Theory. Tech.*, vol. MTT-27, pp. 479–482, May 1979.
[11] Y.-E. Ma and C. Sun, "1-W millimeter-wave Gunn diode combiner," *IEEE Trans. Microwave Theory Tech.*, vol. MTT-28, pp. 1460–1463, Dec. 1980.

[12] K. Kurokawa, "Some basic characteristics of broadband negative resistance oscillator circuits," *Bell Syst. Tech. J.*, vol. 48, pp. 1937–1955, July–Aug. 1969.
[13] C. G. Montgomery, R. H. Dicke, and E. M. Purcell, Eds., *Principles of Microwave Circuits*. New York, NY: McGraw-Hill, 1948, ch. 7, pp. 230–231.

Shigeji Nogi was born in Osaka Prefecture, Japan, on December 26, 1945. He received the B.E., M.E., and D.Eng. degrees in electronics engineering from Kyoto University, Kyoto, Japan, in 1968, 1970, and 1984, respectively.

From 1970 to 1972, he was employed by the Central Research Laboratory, Mitsubishi Electric Corporation, Amagasaki, Japan. In 1972, he joined the Department of Electronics, Okayama University, where he has been engaged in research on microwave active circuits, multimode oscillators, and nonlinear wave propagation.

Dr. Nogi is a member of the Institute of Electronics and Communication Engineers of Japan.

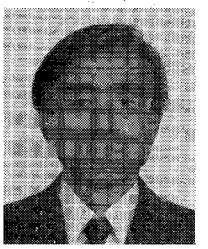

Kiyoshi Fukui (M'75) was born in Tokushima Prefecture, Japan, on January 13, 1930. He received the B.Sc. degree in physics in 1952 and the D.Eng. degree in electronics engineering in 1964 both from Kyoto University, Kyoto, Japan.

From 1958 to 1962, he was a Research Assistant at the Department of Electronics, Kyoto University. From 1962 to 1967, he taught as an Assistant Professor at the Training Institute for Engineering Teachers, Kyoto University. In 1967, he became a Professor of Electronics at the Himeji Institute of Technology, Himeji, Japan. Since 1971, he has been with the Department of Electronics, Okayama University. During 1977–1978, he was on research leave at the University of Wisconsin, Madison. His research interest has been mainly in nonlinear phenomena in electronics such as locking phenomena in oscillators, frequency multiplication by variable capacitance, behavior of multiple-device structures, and nonlinear wave propagation.

Dr. Fukui is a member of the Institute of Electronics and Communication Engineers of Japan and the Physical Society of Japan.

Short Papers

Coaxial E-Field Probe for High-Power Microwave Measurement

S. BURKHART, MEMBER, IEEE

Abstract—**Open-ended semirigid coaxial cable is characterized for use as a coupling element for the measurement of high-power microwaves. There are many high-power microwave experiments where a high vacuum must be maintained, and yet it is necessary to measure the power and frequency of the microwave energy in a cavity or waveguide. Semirigid coaxial cable which is left open-ended and inserted no more than flush with the inner waveguide wall is a convenient way to couple out a known sample of the power. The cable is inserted into the waveguide in a direction parallel to the electric field. The coupling value is expressed in terms of an area multiplier which is applied to the area of the end of the center conductor. The induced charge Q on the center conductor is then determined from $Q = \vec{D} \cdot \hat{n} \cdot$(effective area), and the coupled power is calculated from $P = (\omega Q)^2/(2Z_0)$. For a flush mounted $Z_0 = 50$-Ω coax with a PTFE dielectric, the area multiplier is shown to be 3.846 theoretically and 3.77 experimentally. The area multiplier is also determined for various withdrawal depths of the coax into the waveguide wall.**

I. Introduction

In the measurement of microwaves from short-pulse, high-power microwave generators, the usual quantities desired are output power time history, frequency, and the mode structure. These quantities are typically measured with commercially available couplers, filters, and (< 100-mW) detectors where the generator may be producing > 1 gW of peak power in an overmoded circular waveguide. The primary problem is to sample a small fraction of the power and to transmit the power out of the vacuum region using standard waveguide or coaxial cable to a point where the power and frequency can be measured. The best way to do this is with a directional coupler matched to each mode of interest [1]. But couplers from evacuated circular waveguide into rectangular waveguide are expensive and difficult to fabricate. The time required to fabricate the couplers can also discourage their use. A section of open-ended semirigid cable inserted so that it couples out the radial electric field is described here as a convenient and accurate way to measure E_r and, thus, determine the frequency and power of the assumed mode.

This type of probe is commonly known as an "E-field probe" and is being used as a compact sensor in permittivity studies. For those studies, the effect of dielectrics on the reflection coefficient when the open end of a coaxial cable is inserted into a sample has been modeled by Gajda and Stuchly [2], and by Stuchly *et al.* [3]. However, these models consider power flowing from a generator towards the open end where it is reflected back towards the generator. Here, we address the case where power is coupled into the open end and flows to a matched termination. Smith [4] has done some studies with electrically short coaxial monopoles, but they were fixed length probes, protruding above the metal wall and did not use matched terminations. The E probe we discuss here is inserted into the waveguide through a hole (Fig. 1), yet it is not inserted more than flush with the inner waveguide wall. This makes it possible to leave the outer conductor on the cable, avoiding an additional discontinuity. The cable is vacuum sealed

Manuscript received July 3, 1984; revised October 10, 1984. This work was performed under the auspices of the U.S. Department of Energy by the Lawrence Livermore National Laboratory under Contract W-7405-ENG-48.

The author is with the Electronics Engineering Department, Lawrence Livermore National Laboratory, University of California, P.O. Box 5504, Livermore CA 94550.

0018-9480/85/0300-0262$01.00 ©1985 IEEE